

Effects of Eavesdropper on the Performance of Mixed $\eta - \mu$ and DGG Cooperative Relaying System

NOOR AHMAD SARKER¹, A. S. M. BADRUDDUZA¹, MILTON KUMAR KUNDU², AND IMRAN SHAFIQUE ANSARI³

¹Department of Electronics & Telecommunication Engineering, Rajshahi University of Engineering & Technology (RUET), Rajshahi-6204, Bangladesh

²Department of Electrical & Computer Engineering, RUET, Rajshahi-6204, Bangladesh

³James Watt School of Engineering, University of Glasgow, Glasgow G12 8QQ, United Kingdom

Free-space optical (FSO) channel offers line-of-sight wireless communication with high data rates and high secrecy utilizing unlicensed optical spectrum and also paves the way to the solution of the last-mile access problem. Since atmospheric turbulence is a hindrance to an enhanced secrecy performance, the mixed radio frequency (RF)-FSO system is gaining enormous research interest in recent days. But conventional FSO models except for the double generalized Gamma (DGG) model can not demonstrate secrecy performance for all ranges of turbulence severity. This reason has led us to propose a dual-hop $\eta - \mu$ and unified DGG mixed RF-FSO network while considering eavesdropping at both RF and FSO hops. The security of these proposed scenarios is investigated in terms of two metrics, i.e., strictly positive secrecy capacity and secure outage probability. Exploiting these expressions, we further investigate how the secrecy performance is affected by various system parameters, i.e., fading, turbulence, and pointing errors. A demonstration is made between heterodyne detection (HD) and intensity modulation/direct detection (IM/DD) techniques while exhibiting superior secrecy performance for HD technique over IM/DD technique. Finally, all analytical results are corroborated via Monte-Carlo simulations.

Keywords: Double Generalized Gamma, physical layer security, RF-FSO network, secure outage probability.

1. INTRODUCTION

A. Background and Related Works

In recent years, free-space optical (FSO) communication has gained momentous attention in the field of wireless communication. FSO has many advantages over conventional wireless connection techniques due to its high speed, interference immunity, secured configuration, larger bandwidth, etc. It has also been proven to be a cost-effective wireless system by providing a sufficient amount of license-free spectrum to its users. Meanwhile, having a great potentiality of solving spectrum scarcity complications places FSO as a valuable candidate for wireless technologies in the upcoming era.

Several researches has been performed over FSO systems [1–11] to prove its capability for high speed communication. Authors in [1] investigated the impact of turbulence-induced fading of an FSO network exploiting spatial diversity techniques with multiple receivers. The expression of capacity-vs-outage-probability was derived in [2] at low and high noise regions where simulation results proved the accuracy of those approximations for a moderate number of apertures. Utilizing slow fading conditions, the FSO channel was investigated

in [3] based on the effect of natural turbulence and pointing error. Analysis of capacity for optical wireless communication system was again demonstrated in [4] using maximal ratio combining (MRC) and selective combining (SC) diversity patterns. Investigation of multiple-input-multiple-output (MIMO) FSO channel was performed in [5, 6]. Performance analysis of FSO system using Málaga(\mathcal{M}) turbulence fading was conducted in [7, 8]. As FSO is a short-range communication medium, relaying schemes were applied in many research works [9–11] to increase its communication range. The authors in [9] proposed serial and parallel relaying configuration for both amplify-and-forward (AF) and decode-and-forward (DF) based schemes, and succeeded in mitigating the fading effect. A direct source-to-destination link incorporated with DF relaying system was modeled in [10] where ergodic capacity (EC) was analyzed with respect to the fading parameters. The authors in [11] proposed a two-way relaying (TWR) scheme undergoing double generalized Gamma (DGG) fading.

As FSO medium is highly unfriendly in conveying information signals over a long distance and in non-line-of-sight (NLoS) conditions, the idea of combined radio frequency-free space optical (RF-FSO) communication is brought forward by many researchers [12–38]. This combined communication technique works in such a way that the RF medium covers up the long-distanced path while the FSO medium fills the remaining short portions of that network. For RF link, Rayleigh fading is a popular model used in several RF-FSO research works [12, 14, 15, 17–22]. Authors in [12] proposed a DF-based RF-FSO system and analyzed outage probability (OP), EC, bit error rate (BER), and symbol error rate (SER), and performances exhibiting various modulation schemes. A mixed Rayleigh-Málaga (\mathcal{M}) channel was examined in [14, 15] and novel expressions for cumulative distribution function (CDF) and channel capacity are derived utilizing fixed and variable gain relaying schemes. A TWR scheme was used in [17] with a multi-user theme. A partial relay selection (PRS) scheme for mixed RF-FSO channel was employed in [18] to investigate the outage performance of the system. To minimize fading and turbulence effects in mixed RF-FSO system, a variable-gain relaying scheme is proposed in [19]. Authors in [20] introduced a dual-hop RF-FSO model assembled with hardware impairments that created negligible impact in low signal-to-noise ratio (SNR) regime but the larger impact in high SNR regime. A channel state information (CSI) based RF-FSO system with AF relaying was investigated in [21]. The authors in [22] investigated mixed Rayleigh-(Gamma-Gamma ($\Gamma\Gamma$)) channel with a multi-relaying scheme considering a multi-user perspective. A lot of interest from the researchers is noticed around considering Nakagami- m fading channel at the RF link of mixed RF-FSO channel [24–28, 30, 31]. Authors in [24] proposed a mixed Nakagami- m -Málaga fading channel and investigated OP, average BER (ABER), and EC at high SNRs based on heterodyne detection (HD) and intensity modulation with direct detection (IM/DD) detection techniques at the receiver. A dual-hop AF-based (Nakagami- m)- $\Gamma\Gamma$ fading model was proposed in [25, 26] to investigate OP, EC, and ABER. A combined (Nakagami- m)-DGG system was proposed in [27] where novel expressions for PDF and CDF along with some performance metrics, e.g., OP and ABER were derived. Exact and asymptotic expressions of OP and EC were analyzed in [28]. Ref. [30] introduced a cognitive cooperative RF-FSO model to analyze the outage performance of the system. A generalized fading pair was proposed in [31, 37] showing the effects of atmospheric turbulence, misalignment error, and interference. To gain a better understanding of the mixed RF-FSO link, some researchers introduced generalized fading in RF link [32, 34, 35, 37]. Ref. [32] proposed a mixed $(\eta - \mu) - \Gamma\Gamma$ fading link and analyzed OP, EC, and ABER based on the effects of turbulence and detection types. Identical performance metrics were analyzed in [34] while considering $(\eta - \mu)$ -Málaga combined channel.

Due to the time-varying uncertain nature of the wireless medium, physical layer security (PLS) has always been an important issue. Numerous research has been performed on the secrecy of FSO and mixed RF-FSO networks, as such, [39–51]. The effect of correlation along with the pointing error was analyzed in [39] considering the presence of eavesdropper at the FSO (scenario I) and RF link (scenario II). The authors in [40] investigated PLS over an FSO link experiencing atmospheric turbulence and analyzed the probability of strictly positive secrecy capacity (SPSC). A mixed RF-FSO system was proposed in [41] considering both variable and fixed-gain AF-based relaying where the authors derived the expression of average secrecy capacity (ASC) and secure outage probability (SOP) in both exact and asymptotic forms. PLS for mixed $(\eta - \mu)$ -Málaga channel was studied in [42] where authors analyzed average secrecy rate (ASR) and SOP. A more generalized model is studied in [43] where the authors analyzed the secrecy performance of the system by deriving the expressions

of ASC, SOP, and probability of non-zero secrecy multicast capacity (PNSC). A multi-user-based RF-FSO PLS relaying network was studied in [44] where authors analyzed intercept probability (IP) and SOP in both exact and asymptotic forms. The authors in [45] proposed a secure channel model while considering channel imperfection and analyzed the outage behavior. The SOP was again analyzed in [46] for a mixed RF-FSO simultaneous wireless information and power transfer (SWIPT) downlink system. Another SWIPT model was proposed in [47] for mixed (Nakagami- m)-Málaga single-input-multiple-output (SIMO) channel where authors analyzed ASC and SOP performance. The authors in [48] proposed a DF-based generalized Gamma-Málaga combined channel with a single eavesdropper at the RF link and analyzed ASC, SOP, and SPSC performances. These performance metrics were again analyzed in [49] while considering hyper Gamma(HG)-IT AF-based relaying system model. The authors in [50] analyzed effective secrecy throughput (EST) for mixed RF-FSO secure system while considering imperfect CSI and transmit antenna selection (TAS) patterns. A DF-based secure Rayleigh-IT mixed system was investigated in [51] while considering an eavesdropper at FSO link, where authors analyzed SPSC and lower bound of SOP.

B. Motivation and Contributions

Over the years, researchers have proposed a lot of irradiance models for FSO communication. Although the log-normal model is one of the most popular models for its simplicity, it is appropriate for only weak turbulence conditions [52] while facing tractability issues. Recently, the Gamma-Gamma channel model is being utilized for FSO channel modeling quite extensively but a study in [53] reveals that the double Weibull channel model exhibits more superiority, specifically for moderate and strong turbulence conditions. Hence, for the purpose of unification, in [54], the author proposed a double generalized Gamma (DGG) model that addresses weak to strong turbulence conditions and eliminates the pitfalls of all other existing FSO channel models. Besides, it is also noted that the PLS analysis while considering generalized fading models in both FSO and RF hops is also infrequent. Moreover, most of the works consider eavesdropper's placement at only the RF or FSO hops and also PLS analysis over the DGG model has not been reported in the literature yet that indicates a large research gap in secrecy analysis over FSO channels applicable in all atmospheric turbulence conditions. Hence, in our proposed RF-FSO system, we consider two generalized fading models namely $\eta - \mu$ and DGG fadings in the RF and FSO hops, respectively. We also consider two eavesdropping scenarios i.e. at the RF and FSO hops. Our main contributions in this work are summarized below:

1. We first derive the CDF and PDF of the considered dual-hop RF-FSO system via utilizing the CDF and PDF of the SNR of each individual hop. To the best of the authors' knowledge, these expressions possess novelty over other existing systems [32, 41] as both of our proposed fading channels (RF and FSO) convey generic fading characteristics [54, 55].
2. We analyze the secrecy performance of the considered system via deducing expressions of two secrecy performance metrics, i.e., SOP and SPSC applicable in two different eavesdropping scenarios. The analytical outcomes are further validated via Monte-Carlo (MC) simulations. Besides, we also derive the asymptotic SOP expression to acquire more insightful observations on the secure outage performance. Although the authors in [41, 42, 44–51] proposed similar secure systems, we obtain superiority in our analysis over these researches since the proposed models in this work can analyze the secrecy performance overall turbulence conditions. Also, we demonstrate the results presented in [41, 44, 51] can be directly achieved as special cases of our work.
3. We also demonstrate selected analytical outcomes while utilizing system performance metrics showing impacts of the fading parameters of RF channel, atmospheric turbulence, pointing errors, etc. Besides, we also investigate HD and IM/DD techniques to demonstrate the supremacy of the HD technique over the IM/DD technique.

C. Organization

The remaining parts of this work are arranged as follows. Section II presents the system model and formulation of its CDF expressions. Novel expressions for the SOP and SPSC are derived in Section III. Section IV

demonstrates the numerical results of our deduced secrecy metrics. Finally, concluding remarks are provided in Section V.

2. SYSTEM MODEL AND PROBLEM FORMULATION

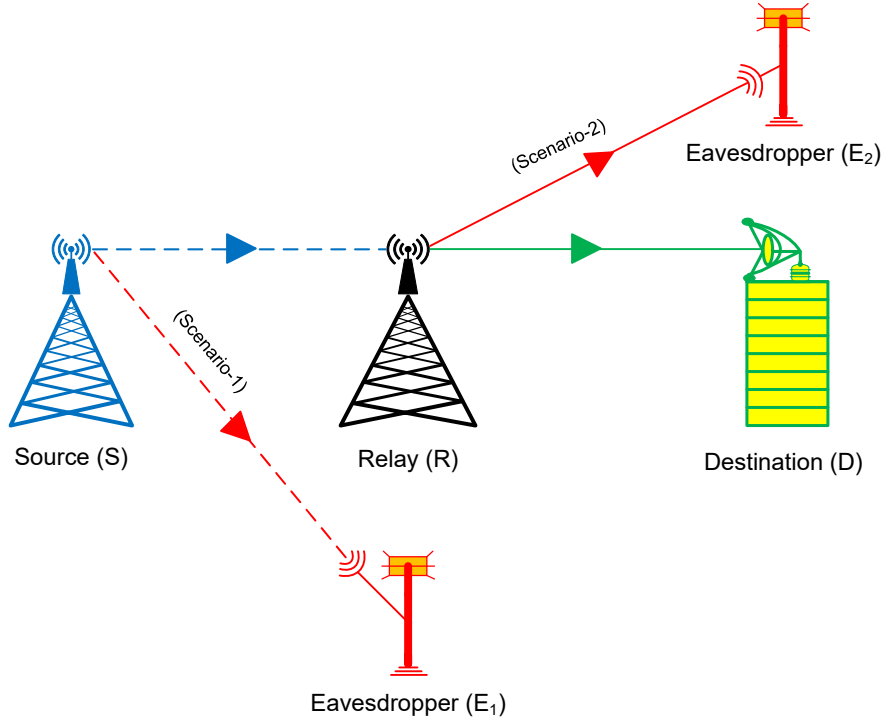


Fig. 1. System model incorporating the source (S), relay (R), two eavesdroppers (E_1 and E_2), and destination (D).

We consider a combined RF-FSO system presented in Fig. 1, where information is transmitted from source S to destination D through a passable medium relay R , where R converts the radio waves into optical waves. We consider DF-based relaying scheme for our proposed system. S consists of one transmitting antenna, R houses one receive antenna and one transmit aperture, and D has an aperture to receive the transmitted optical wave from the relay. The link between S and R is a RF link that is experiencing $\eta - \mu$ fading. On the other hand, $R - D$ link is connected via FSO DGG fading channel. According to the eavesdropper's position, we consider the communication process with experience under the following two scenarios:

- **Scenario-1:** Eavesdropper E_1 tries to intercept confidential data transferred through $S - R$ link via another $\eta - \mu$ link. The $R - D$ FSO link is safe from this eavesdropping. Herein, we consider E_1 consists of one receive antenna.
- **Scenario-2:** The first hop ($S - R$ link) is totally secure while eavesdropper E_2 tries to eavesdrop confidential information from $R - D$ link via another DGG fading FSO ($R - E_2$) link. Herein, we assume E_2 houses one receive aperture.

A. SNR of Each Link

For main RF-FSO channel, we represent γ_{r_0} and γ_{d_0} as the instantaneous SNRs of $S - R$ and $R - D$ hops, respectively. For eavesdropper channels, γ_{r_e} and γ_{d_e} are denoted as the instantaneous SNRs of $S - E_1$ link (Scenario-1) and $R - E_2$ link (Scenario-2), respectively. We can mathematically express these SNRs as $\gamma_{r_0} =$

$\phi_{s,r} \|\alpha_{s,r}\|^2$, $\gamma_{r_e} = \phi_{s,e} \|\alpha_{s,e}\|^2$, $\gamma_{d_0} = \phi_{r,d} \|\alpha_{r,d}\|^2$, and $\gamma_{d_e} = \phi_{r,e} \|\alpha_{r,e}\|^2$, where $\phi_{s,r}$, $\phi_{s,e}$, $\phi_{r,d}$, and $\phi_{r,e}$ denote the average SNRs while $\alpha_{s,r}$, $\alpha_{s,e}$, $\alpha_{r,d}$, and $\alpha_{r,e}$ denote the corresponding channel gains of the $S - R$, $S - E_1$, $R - D$, and $R - E_2$ links, respectively. For combined $S - R - D$ link, R is utilized for assisting in relaying purpose with the help of channel state information. By considering this fact, SNR of $S - R - D$ and $S - R - E_2$ link is defined as [Eq. (5), 56]

$$\gamma_d = \min \{ \gamma_{r_0}, \gamma_{d_0} \}, \quad (1a)$$

$$\gamma_e = \min \{ \gamma_{r_0}, \gamma_{d_e} \}. \quad (1b)$$

B. Secrecy Capacity

To ensure secure and reliable transmission of information between S and D , we need to maintain a rate at which the eavesdropper is unable to wiretap the confidential transmitted data that is known as secrecy rate. To confirm secure transmission for the considered dual-hop communication system in Fig. 1, the definition of secrecy capacity (SC) for both scenarios is given below.

B.1. Instantaneous SC for Scenario-1

Considering the first scenario where eavesdropper E_1 tries to eavesdrop the data from S while experiencing $\eta - \mu$ fading over its link, the instantaneous SC for dual-hop transmission model is defined as [Eq. (3), 57]

$$\mathcal{T}_{D_1} = \begin{cases} \log_2(1 + \gamma_d) - \log_2(1 + \gamma_{r_e}), & \text{if } \gamma_d > \gamma_{r_e} \\ 0, & \text{if } \gamma_d \leq \gamma_{r_e}. \end{cases} \quad (2)$$

B.2. Instantaneous SC for Scenario-2

In the second scenario of Fig. 1 where the eavesdropper E_2 tries to eavesdrop the data being transmitted from R , two SCs are considered for the two hops (i.e. $S - R$ and $R - D$). As $S - R$ link is not affected by E_2 , instantaneous SC for this link is defined as

$$\mathcal{T}_S = \frac{1}{2} \log_2(1 + \gamma_{r_0}). \quad (3)$$

For $R - D$ link where data transmission is affected by $R - E_2$ eavesdropper link, instantaneous SC is defined as

$$\mathcal{T}_R = \left[\frac{1}{2} (\log_2(1 + \gamma_{d_0}) - \log_2(1 + \gamma_{d_e})) \right]^+, \quad (4)$$

where $[f]^+ = \max \{f, 0\}$. As *scenario-2* in Fig. 1 contains DF based relaying, this system is similar to a series configuration where the worst hop acts as the dominating contributor to secrecy capacity of the system. So, the instantaneous SC for the system in Fig. 1 (*scenario-2*) is defined as [Eq. (13), 58]

$$\mathcal{T}_{D_2} = \min(\mathcal{T}_S, \mathcal{T}_R). \quad (5)$$

C. PDF and CDF of SNR for RF Main Channel

Considering $\eta - \mu$ fading distribution effecting the main RF channel (i.e. $S - R$ link), the PDF of γ_{r_0} can be given by [Eq. (3), 59]

$$f_{\gamma_{r_0}}(\gamma) = \mathcal{M}_1 \gamma^{\mu_0 - \frac{1}{2}} e^{-\mathcal{M}_2 \gamma} I_{\mu_0 - \frac{1}{2}}(\mathcal{M}_3 \gamma), \quad (6)$$

where $\mathcal{M}_1 = \frac{2\sqrt{\pi}\mu_0^{\mu_0 + \frac{1}{2}}k_0^{\mu_0}}{\Gamma(\mu_0)K_0^{\mu_0 - \frac{1}{2}}\phi_{s,r}^{\mu_0 + \frac{1}{2}}}$, $\mathcal{M}_2 = \frac{2k_0\mu_0}{\phi_{s,r}}$, and $\mathcal{M}_3 = \frac{2K_0\mu_0}{\phi_{s,r}}$. Both parameters k_0 and K_0 can be explained as $k_0 = \frac{2+\eta_0^{-1}+\eta_0}{4}$ and $K_0 = \frac{\eta_0^{-1}-\eta_0}{4}$. To satisfy these expressions of k_0 and K_0 applicable to main RF channel, the range of η_0 is fixed as $0 < \eta_0 < \infty$ [55, 60]. Parameter μ_0 represents the fading signal envelope of $S - R$ link with $\mu_0 > 0$ and $\Gamma(\cdot)$ represents Gamma operator [Eq. (8.310) 61]. $\eta - \mu$ fading distribution has unique generic

Table 1. Special Cases of $\eta - \mu$ Fading Distribution Channel [55].

Channels	$\eta - \mu$ Distribution Parameters
Hoyt / Nakagami- q	$\eta = q^2, \mu = 0.5$
One-sided Gaussian	$\eta \rightarrow 0$ (or $\eta \rightarrow \infty$), $\mu = 0.5$
Rayleigh	$\eta \rightarrow 0$ (or $\eta \rightarrow \infty$), $\mu = 1$
Nakagami- m	$\eta \rightarrow 0$ (or $\eta \rightarrow \infty$), $\mu = m$

characteristics that allows it to represent several multipath fading channels as listed in Table 1. Since the value of μ is considered as integer in most of the works [42], Eq. (6) is rewritten as

$$f_{\gamma_{r_0}}(\gamma) = \mathcal{A} \sum_{N_0=1}^2 \sum_{v=0}^{\mu_0-1} X_{N_0,v} \gamma^{\mu_0-v-1} e^{-l_{N_0} \gamma}, \quad (7)$$

where $\mathcal{A} = \frac{k_0^{\mu_0}}{K_0^{\mu_0} \Gamma(\mu_0)}$, $X_{1,v} = \frac{\Gamma(\mu_0+v)(\mu_0)^{\mu_0-v}}{v! \Gamma(\mu_0-v) 4^v \phi_{s,r}^{\mu_0-v} K_0^v} (-1)^v$, $X_{2,v} = \frac{\Gamma(\mu_0+v)(\mu_0)^{\mu_0-v}}{v! \Gamma(\mu_0-v) 4^v \phi_{s,r}^{\mu_0-v} K_0^v} (-1)^{\mu_0}$, $l_1 = \frac{2\mu_0(k_0-K_0)}{\phi_{s,r}}$, and $l_2 = \frac{2\mu_0(k_0+K_0)}{\phi_{s,r}}$. The CDF of γ_{r_0} can be expressed as [Eq. (4), 42]

$$F_{\gamma_{r_0}}(\gamma) = 1 - \mathcal{A} \sum_{N_0=1}^2 \sum_{v=0}^{\mu_0-1} \sum_{x=0}^{\mu_0-v-1} \frac{\gamma^x}{x!} e^{-l_{N_0} \gamma} l_{N_0}^x Y_{N_0,v}, \quad (8)$$

where $Y_{1,v} = \frac{\Gamma(\mu_0+v)(-1)^v K_0^{-v}}{v! 2^{\mu_0+v} (k_0-K_0)^{\mu_0-v}}$, and $Y_{2,v} = \frac{\Gamma(\mu_0+v)(-1)^{\mu_0} K_0^{-v}}{v! 2^{\mu_0+v} (k_0+K_0)^{\mu_0-v}}$.

D. PDF and CDF of SNR for FSO Main Channel

Considering DGG fading experience over our proposed FSO hop, the PDF of $R - D$ link is defined as [Eq. (12), 52]

$$f_{\gamma_{d_0}}(\gamma) = \frac{\mathcal{B}_1}{s_0 \gamma} G_{1, \lambda_1 + \lambda_2 + 1}^{\lambda_1 + \lambda_2 + 1, 0} \left[\mathcal{B}_2 t^\tau \left(\frac{\gamma}{U_d} \right)^{\frac{\tau}{s_0}} \middle| \begin{matrix} j_2 \\ j_1 \end{matrix} \right], \quad (9)$$

where $\mathcal{B}_1 = \frac{\epsilon^2 \lambda_2^{b_1 - \frac{1}{2}} \lambda_1^{b_2 - \frac{1}{2}} (2\pi)^{1 - \frac{\lambda_1 + \lambda_2}{2}}}{\Gamma(b_1) \Gamma(b_2)}$, $\mathcal{B}_2 = \frac{b_1^{\lambda_2} b_2^{\lambda_1}}{\lambda_1^{\lambda_1} \lambda_2^{\lambda_2} \Omega_1^{\lambda_2} \Omega_2^{\lambda_1}}$, $t = \frac{\mathcal{B}_1 \zeta}{(1 + \epsilon^2) \mathcal{B}_2^{\frac{1}{a_2 \lambda_1}}}$, and $\tau = a_2 \lambda_1$. The values of a_1 , a_2 , Ω_1 ,

and Ω_2 are mathematically calculated that are identified by the variances related to large-scale and small-scale fluctuations [62]. The two shaping parameters b_1 and b_2 define fading characteristics induced via turbulence conditions [54]. Two positive integers λ_1 and λ_2 are defined such that $\frac{\lambda_1}{\lambda_2} = \frac{a_1}{a_2}$ [52], s_0 represents two types of detections utilized at D for receiving optical signals ($s_0 = 1$ symbolizes HD technique and $s_0 = 2$ represents IM/DD technique), and ϵ acts as the indicator for pointing error in the FSO channel that is actually a ratio between the width of equivalent signal beam and the jitter of pointing error displacement [8]. The electrical SNR for DGG fading model over $R - D$ link is defined as $U_d = \frac{\{\Lambda_0 E[I_0]\}^{s_0}}{P_0}$, respectively. Here, Λ_0 , I_0 , and P_0 denote photoelectric conversion coefficient, receiver irradiance, and number of sample apertures, respectively [63]. Hence, the trivial relationship between $\phi_{r,d}$ and U_d can be addressed as $\frac{E[I_0^2]}{E[I_0]^2} \triangleq i_0^2 + 1$, where i_0^2 represents the scintillation index [64]. Parameter ζ is expressed as $\zeta = \prod_{i=1}^{\lambda_1 + \lambda_2} \Gamma(\frac{1}{a_2 \lambda_1} + \Psi_i)$, where Ψ_q denotes the q -th

term of Ψ [52]. The terms Ψ , j_1 , and j_2 are expressed as

$$\begin{aligned}\Psi &= \Delta(\lambda_2 : b_1), \Delta(\lambda_1 : b_2), \\ j_1 &= \frac{\epsilon^2}{a_2 \lambda_1}, \Delta(\lambda_2 : b_1), \Delta(\lambda_1 : b_2), \\ j_2 &= \frac{a_2 \lambda_1 + \epsilon^2}{a_2 \lambda_1},\end{aligned}$$

and the symbol notation $\Delta(p : q)$ including p terms is defined as

$$\Delta(p : q) = \frac{q}{p}, \frac{q+1}{p}, \dots, \frac{q+p-1}{p}.$$

The DGG turbulence model is a generic fading model for FSO communications thereby housing several classical fading models within itself as listed in Table 2. Hence, this is one of the most popular fading model

Table 2. Special Cases of DGG Turbulence Fading Channel [54].

Channels	DGG turbulence parameters
Double-Weibull	$b_1 = b_2 = 1$
$\Gamma\Gamma$	$a_1 = a_2 = \Omega_1 = \Omega_2 = 1$
Lognormal	$a_1 \rightarrow 0, a_2 \rightarrow 0, b_1 \rightarrow \infty, b_2 \rightarrow \infty$
K distribution	$a_1 = a_2 = b_2 = \Omega_1 = \Omega_2 = 1$

that has attracted many OWC researchers. Moreover, the CDF of γ_{d_0} is defined as [Eq. (14), 52]

$$F_{\gamma_{d_0}}(\gamma) = \mathcal{B}_3 G_{s_0+1, \delta_0+1}^{\delta_0, 1} \left[\mathcal{B}_4 \left(\frac{\gamma}{U_d} \right)^\tau \middle| 1, j_3 \right]_{j_4, 0}, \quad (10)$$

where $\mathcal{B}_3 = \frac{\epsilon^2 \lambda_2^{b_1 - \frac{1}{2}} \lambda_1^{b_2 - \frac{1}{2}} (2\pi)^{1 - \frac{s_0(\lambda_1 + \lambda_2)}{2}} s_0^{b_1 + b_2 - 2}}{a_2 \lambda_1 \Gamma(b_1) \Gamma(b_2)}$, $\mathcal{B}_4 = \left(\frac{\mathcal{B}_2 \mu_2^{\lambda_1}}{s_0^{\lambda_1 + \lambda_2}} \right)^{s_0}$, and $\delta_0 = s_0(\lambda_1 + \lambda_2 + 1)$. The series terms $j_3 = [\Delta(s_0 : j_2)]$ and $j_4 = [\Delta(s_0 : j_1)]$ are denoted comprising of s_0 and δ_0 terms, respectively, where the series expression $[\Delta(\sigma : \mathcal{L}_z)]$ with z terms is defined as

$$[\Delta(\sigma : \mathcal{L}_z)] = \Delta(\sigma : \mathcal{L}_1), \Delta(\sigma : \mathcal{L}_2), \dots, \Delta(\sigma : \mathcal{L}_z). \quad (11)$$

E. PDF and CDF of SNR for the Eavesdropper Channels

E.1. Eavesdropper at the RF link

Similar to the main RF channel, the PDF of SNR for $S - E_1$ link can be defined as [Eq. (3), 59]

$$f_{\gamma_{re}}(\gamma) = \mathcal{C} \sum_{N_e=1}^2 \sum_{w=0}^{\mu_e-1} X_{N_e, w} \gamma^{\mu_e-w-1} e^{-l_{N_e} \gamma}, \quad (12)$$

where $\mathcal{C} = \frac{k_e^{\mu_e}}{K_e^{\mu_e} \Gamma(\mu_e)}$, $X_{1, w} = \frac{\Gamma(\mu_e + w) \mu_e^{\mu_e - w}}{w! \Gamma(\mu_e - w) 4^w \phi_{s, e}^{\mu_e - w} K_e^w} (-1)^w$, $X_{2, w} = \frac{\Gamma(\mu_e + w) \mu_e^{\mu_e - w}}{w! \Gamma(\mu_e - w) 4^w \phi_{s, e}^{\mu_e - w} K_e^w} (-1)^{\mu_e}$, $l_1 = \frac{2\mu_e(k_e - K_e)}{\phi_{s, e}}$, and $l_2 = \frac{2\mu_e(k_e + K_e)}{\phi_{s, e}}$. Considering the specific condition of $0 < \eta_e < \infty$, parameters k_e and K_e are denoted as $k_e = \frac{2+\eta_e^{-1}+\eta_e}{4}$ and $K_e = \frac{\eta_e^{-1}-\eta_e}{4}$. Parameter $\mu_e > 0$ denotes the fading of $S - E_1$ channel. Similar to Eq. (8), CDF of γ_{re} is expressed as [Eq. (4), 42]

$$F_{\gamma_{re}}(\gamma) = 1 - \mathcal{C} \sum_{N_e=1}^2 \sum_{w=0}^{\mu_e-1} \sum_{y=0}^{\mu_e-w-1} \frac{\gamma^y}{y!} e^{-l_{N_e} \gamma} l_{N_e}^y Y_{N_e, w}, \quad (13)$$

where $Y_{1,w} = \frac{\Gamma(\mu_e+w)(-1)^w K_e^{-w}}{w!2^{\mu_e+w}(k_e-K_e)^{\mu_e-w}}$, and $Y_{2,w} = \frac{\Gamma(\mu_e+w)(-1)^{\mu_e} K_e^{-w}}{w!2^{\mu_e+w}(k_e+K_e)^{\mu_e-w}}$.

E.2. Eavesdropper at the FSO link

The $R - E_2$ link experiences DGG fading similar to main FSO link, the PDF of γ_{d_e} is defined as [Eq. (12), 52]

$$f_{\gamma_{d_e}}(\gamma) = \frac{\mathcal{B}_1}{s_e \gamma} G_{1, \lambda_1 + \lambda_2 + 1}^{\lambda_1 + \lambda_2 + 1, 0} \left[\mathcal{B}_2 t^\tau \left(\frac{\gamma}{U_e} \right)^{\frac{\tau}{s_e}} \middle| \begin{matrix} j_2 \\ j_1 \end{matrix} \right], \quad (14)$$

where s_e represents the two detection types through which E_2 receives the optical signals ($s_e = 1$ denotes HD technique and $s_e = 2$ denotes IM/DD technique). As in Eq. (9), all parameters of DGG fading model related to atmospheric turbulence and pointing error are similar for both FSO main and eavesdropper channels. The electrical SNR of this link is addressed as $U_e = \frac{\{\Lambda_e E[I_e]\}^{s_e}}{P_e}$. Here, Λ_e , I_e , and P_e denote photoelectric conversion coefficient, receiver irradiance, and number of sample apertures, respectively, for $R - E_2$ link. As a result, $\frac{E[I_e^2]}{E[I_e]^2} \triangleq \iota_e^2 + 1$ indicates the trivial relationship between $\phi_{r,e}$ and U_e , where ι_e^2 is the scintillation index for $R - E_2$ link. Similar to Eq. (10), CDF of γ_{d_e} is defined as [Eq. (14), 52]

$$F_{\gamma_{d_e}}(\gamma) = \mathcal{B}_5 G_{s_e+1, \delta_e+1}^{\delta_e, 1} \left[\mathcal{B}_6 \left(\frac{\gamma}{U_e} \right)^\tau \middle| \begin{matrix} 1, j_5 \\ j_6, 0 \end{matrix} \right], \quad (15)$$

where $\mathcal{B}_5 = \frac{\epsilon^2 \lambda_2^{b_1 - \frac{1}{2}} \lambda_1^{b_2 - \frac{1}{2}} (2\pi)^{1 - \frac{s_e(\lambda_1 + \lambda_2)}{2}} s_e^{b_1 + b_2 - 2}}{a_2 \lambda_1 \Gamma(b_1) \Gamma(b_2)}$, $\mathcal{B}_6 = \left(\frac{\mathcal{B}_2 t^{a_2 \lambda_1}}{s_e^{\lambda_1 + \lambda_2}} \right)^{s_e}$, and $\delta_e = s_e(\lambda_1 + \lambda_2 + 1)$. The series terms $j_5 = [\Delta(s_e : j_2)]$ and $j_6 = [\Delta(s_e : j_1)]$ comprise of s_e and δ_e terms, respectively, and are symbolized according to Eq. (11).

F. PDF and CDF of SNR for Dual-hop RF-FSO Link

Utilizing order statistics, the CDF of γ_d is expressed as [Eq. (5), 26]

$$\begin{aligned} F_{\gamma_d}(\gamma) &= \Pr[\min(\gamma_{r_0}, \gamma_{d_0}) < \gamma] \\ &= F_{\gamma_{r_0}}(\gamma) + F_{\gamma_{d_0}}(\gamma) - F_{\gamma_{r_0}}(\gamma)F_{\gamma_{d_0}}(\gamma). \end{aligned} \quad (16)$$

Placing Eq. (8) and Eq. (10) into Eq. (16) and performing some arithmetic simplifications, the CDF of γ_d is written as

$$F_{\gamma_d}(\gamma) = 1 - \mathcal{A} \sum_{N_0=1}^2 \sum_{v=0}^{\mu_0-1} \sum_{x=0}^{\mu_0-v-1} \frac{\gamma^x}{x!} e^{-I_{N_0} \gamma} I_{N_0}^x Y_{N_0, v} \left\{ 1 - \mathcal{B}_3 G_{s_0+1, \delta_0+1}^{\delta_0, 1} \left[\mathcal{B}_4 \left(\frac{\gamma}{U_d} \right)^\tau \middle| \begin{matrix} 1, j_3 \\ j_4, 0 \end{matrix} \right] \right\}. \quad (17)$$

The PDF of γ_d is defined as [Eq. (4), 12]

$$f_{\gamma_d}(\gamma) = f_{\gamma_{r_0}}(\gamma) + f_{\gamma_{d_0}}(\gamma) - f_{\gamma_{r_0}}(\gamma)F_{\gamma_{d_0}}(\gamma) - f_{\gamma_{d_0}}(\gamma)F_{\gamma_{r_0}}(\gamma). \quad (18)$$

Substituting Eq. (7), Eq. (8), Eq. (9), and Eq. (10) into Eq. (18) and doing some simplifications, the PDF of γ_d is obtained as

$$\begin{aligned} f_{\gamma_d}(\gamma) &= \mathcal{A} \sum_{N_0=1}^2 \sum_{v=0}^{\mu_0-1} e^{-I_{N_0} \gamma} \left\{ \frac{\mathcal{B}_1}{s_0} \sum_{x=0}^{\mu_0-v-1} \frac{I_{N_0}^x}{x!} \gamma^{x-1} Y_{N_0, v} G_{1, \lambda_1 + \lambda_2 + 1}^{\lambda_1 + \lambda_2 + 1, 0} \left[\mathcal{B}_2 t^\tau \left(\frac{\gamma}{U_d} \right)^{\frac{\tau}{s_0}} \middle| \begin{matrix} j_2 \\ j_1 \end{matrix} \right] \right. \\ &\quad \left. + \mathcal{B}_3 X_{N_0, v} G_{s_0+1, \delta_0+1}^{s_0+1, 0} \left[\mathcal{B}_4 \left(\frac{\gamma}{U_d} \right)^\tau \middle| \begin{matrix} j_3, 1 \\ 0, j_4 \end{matrix} \right] \right\}. \end{aligned} \quad (19)$$

3. PERFORMANCE ANALYSIS

In this section, we derive novel closed-form expressions of SOP and SPSC for both the proposed scenarios. We also derive asymptotic expressions for SOP to obtain better intuition on our analysis.

A. Secure Outage Probability

SOP is a decisive performance metric for secrecy analysis. It demonstrates the reverse mechanism to evaluate secrecy performance. For both *scenario-1* and *scenario-2* of our proposed model, we derive two different SOP expressions based on different positions of the eavesdropper.

A.1. Scenario-1

Considering \mathcal{T}_{C_1} as the target secrecy rate for *scenario-1*, the occurrence of an outage event for secrecy measurement can be defined when \mathcal{T}_{D_1} falls below \mathcal{T}_{C_1} . According to this theory, SOP for RF-FSO combined system in *scenario-1* can be introduced as [Eq. (14), 65]

$$\begin{aligned} \text{SOP}_1 &= \Pr \{ \mathcal{T}_{D_1} \leq \mathcal{T}_{C_1} \} \\ &= \Pr \{ \gamma_d \leq \varphi_1 \gamma_{re} + \varphi_1 - 1 \}. \end{aligned} \quad (20)$$

where $\varphi_1 = 2^{\mathcal{T}_{C_1}}$. The term in Eq. (20) can be described as [66, 67]

$$\begin{aligned} \text{SOP}_1 &= 1 - \int_0^\infty \int_{\varphi_1 \gamma_{re} + \varphi_1 - 1}^\infty f_d(\gamma_d) f_{re}(\gamma_{re}) d\gamma_d d\gamma_{re} \\ &= \int_0^\infty F_{\gamma_d}(\varphi_1 \gamma + \varphi_1 - 1) f_{\gamma_{re}}(\gamma) d\gamma, \end{aligned} \quad (21)$$

Although the expression defined in Eq. (21) is the exact expression of SOP, solving Eq. (21) in closed-form is not possible due to mathematical complexities. Hence, for DF relaying scheme, we often consider lower-bound SOP as [Eq. (6), 68]

$$\text{SOP}_1 \geq \text{SOP}_{1,L} = \int_0^\infty F_{\gamma_d}(\varphi_1 \gamma) f_{\gamma_{re}}(\gamma) d\gamma. \quad (22)$$

Substituting Eq. (12) and Eq. (17) into Eq. (22), the SOP for *scenario-1* is expressed as

$$\text{SOP}_{1,L} = 1 - \mathcal{AC} \sum_{N_0=1}^2 \sum_{N_e=1}^2 \sum_{v=0}^{\mu_0-1} \sum_{w=0}^{\mu_e-1} \sum_{x=0}^{\mu_0-v-1} \frac{l_{N_0}^x}{x!} X_{N_e, w} Y_{N_0, v} (Q_1 - \mathcal{B}_3 Q_2). \quad (23)$$

Performing integration operation utilizing [Eq. (3.351.3), 61], the term Q_1 in Eq. (23) is obtained as

$$\begin{aligned} Q_1 &= \int_0^\infty \gamma_{re}^{z_1-1} e^{-\mathcal{F} \gamma_{re}} \varphi_1^x d\gamma_{re} \\ &= \frac{\varphi_1^x \Gamma(z_1)}{(\mathcal{F})^{z_1}}, \end{aligned} \quad (24)$$

where $\mathcal{F} = \varphi_1 l_{N_0} + l_{N_e}$, and $z_1 = \mu_e - w + x$. Subsequently, converting the exponential term to Meijer's G function and then performing integration via applying [eqs. (2.24.1.1) and (8.4.3.1), 69], the term Q_2 in Eq. (23) is obtained as

$$\begin{aligned} Q_2 &= \int_0^\infty \gamma_{re}^{z_1-1} \varphi_1^x e^{-\mathcal{F} \gamma_{re}} G_{s_0+1, \delta_0+1}^{\delta_0, 1} \left[\mathcal{B}_4 \left(\frac{\varphi_1 \gamma_{re}}{U_d} \right)^\tau \middle| \begin{matrix} 1, j_3 \\ j_4, 0 \end{matrix} \right] d\gamma_{re} \\ &= \int_0^\infty \gamma_{re}^{z_1-1} \varphi_1^x G_{0,1}^{1,0} \left[\mathcal{F} \gamma_{re} \middle| \begin{matrix} - \\ 0 \end{matrix} \right] G_{s_0+1, \delta_0+1}^{\delta_0, 1} \left[\mathcal{B}_4 \left(\frac{\varphi_1 \gamma_{re}}{U_d} \right)^\tau \middle| \begin{matrix} 1, j_3 \\ j_4, 0 \end{matrix} \right] d\gamma_{re} \\ &= \frac{\varphi_1^x}{\mathcal{F}^{z_1}} G_{s_0+2, \delta_0+1}^{\delta_0, 2} \left[\mathcal{B}_4 \left(\frac{\varphi_1 \tau}{U_d \mathcal{F}} \right)^\tau \middle| \begin{matrix} 1, 1 - z_1, j_3 \\ j_4, 0 \end{matrix} \right]. \end{aligned} \quad (25)$$

The expression in Eq. (23) can be utilized to obtain Rayleigh- $\Gamma\Gamma$ distribution [Eq. (15), 44] by setting $\eta_0 = \eta_e = 1$, $\mu_0 = \mu_e = 1$, $a_1 = a_2 = \Omega_1 = \Omega_2 = 1$. It can also be reformed as (Nakagami- m)- $\Gamma\Gamma$ distribution [Eq. (13), 41] via setting $\eta_0 \geq 1$, $\eta_e \geq 1$, $\mu_0 \geq 1$, $\mu_e \geq 1$, and $a_1 = a_2 = \Omega_1 = \Omega_2 = 1$.

Asymptotic Expression:

To gain better understanding of the secrecy incident of our proposed model, we derive asymptotic SOP expression by setting $U_d \rightarrow \infty$. By converting the Meijer's G term described in Eq. (23) via utilizing [Eq. (6.2.2), 70] and [Eq. (19), 8], the asymptotic SOP for *scenario-1* is expressed as

$$SOP_{1,\infty} = 1 - \mathcal{AC} \sum_{N_0=1}^2 \sum_{N_e=1}^2 \sum_{v=0}^{\mu_0-1} \sum_{w=0}^{\mu_e-1} \sum_{x=0}^{\mu_0-v-1} \frac{l_{N_0}^x}{x!} X_{N_e,w} Y_{N_0,v} \times \left[Q_1 - \frac{\mathcal{B}_3 \varphi_1^x}{\mathcal{F}^{z_1}} \sum_{p=1}^{\delta_0} \Gamma(j_{4,p}) \mathcal{B}_4^{j_{4,p}} \frac{\prod_{h=1, h \neq p}^{\delta_0} \Gamma(j_{4,h} - j_{4,p})}{\prod_{h=3}^{\delta_0+2} \Gamma(j_{3,h} - j_{4,p})} \left(\frac{U_d \mathcal{F}}{\varphi_1 \tau} \right)^{-\tau j_{4,p}} \right]. \quad (26)$$

A.2. scenario-2

For the DF based relaying configuration setup in *scenario-2* of Fig. 1, SOP is defined as

$$SOP_2 = \Pr \{ \mathcal{T}_{D_2} < \mathcal{T}_{C_2} \}, \quad (27)$$

where T_{C_2} is defined as the target SC for second scenario of our proposed model. As the model explained in *scenario-2* is autonomous and links RF-FSO relaying system, SOP for this case can be defined by substituting Eq. (5) into Eq. (27) as

$$\begin{aligned} SOP_2 &= \Pr \{ \min(\mathcal{T}_S, \mathcal{T}_R) < T_{C_2} \} \\ &= 1 - \Pr \{ \min(\mathcal{T}_S, \mathcal{T}_R) \geq T_{C_2} \} \\ &= 1 - \Pr \{ \mathcal{T}_S \geq T_{C_2} \} \Pr \{ \mathcal{T}_R \geq T_{C_2} \}. \end{aligned} \quad (28)$$

Substituting the values of Eq. (8), Eq. (10), and Eq. (14) into Eq. (28), we have

$$SOP_2 = \int_0^\infty F_{\gamma_{d_0}}(\varphi_2 \gamma + \varphi_2 - 1) f_{\gamma_{d_e}}(\gamma) \left\{ 1 - F_{\gamma_{r_0}}(\varphi_2 - 1) \right\} d\gamma + F_{\gamma_{r_0}}(\varphi_2 - 1), \quad (29)$$

where $\varphi_2 = 2^{2T_{C_2}}$. For defining closed-form expression, we must delineate the lower bound of SOP, similar to Eq. (22), as

$$SOP_2 \geq SOP_{2,L} \cong \int_0^\infty F_{\gamma_{d_0}}(\varphi_2 \gamma) f_{\gamma_{d_e}}(\gamma) \left\{ 1 - F_{\gamma_{r_0}}(\varphi_2 - 1) \right\} d\gamma + F_{\gamma_{r_0}}(\varphi_2 - 1). \quad (30)$$

Placing Eq. (8), Eq. (10), and Eq. (14) into Eq. (30) and performing some integration and simplifications via utilizing [Eq. (2.24.1.1), 69], Eq. (30) is obtained as

$$\begin{aligned} SOP_{2,L} &= 1 - \mathcal{A} \sum_{N_0=1}^2 \sum_{v=0}^{\mu_0-1} \sum_{x=0}^{\mu_0-v-1} \frac{(\varphi_2 - 1)^x}{x!} e^{-l_{N_0}(\varphi_2-1)} l_{N_0}^x Y_{N_0,v} \\ &\quad \times \left\{ 1 - \mathcal{B}_3 \mathcal{B}_5 G_{s_e+\delta_0+1, s_0+\delta_e+1}^{\delta_e+1, \delta_0} \left[\frac{\mathcal{B}_6}{\mathcal{B}_4} \left(\frac{U_d}{U_e \varphi_2} \right)^\tau \middle| \begin{matrix} 1-j_4, 1, j_5 \\ j_6, 0, 1-j_3 \end{matrix} \right] \right\}. \end{aligned} \quad (31)$$

It is observed that the derived expression in Eq. (31) can be utilized to generate Rayleigh- $\Gamma\Gamma$ distribution [Eq. (19), 51] while considering the conditions $\eta_0 = 1$, and $\mu_0 = 1$, $a_1 = a_2 = \Omega_1 = \Omega_2 = 1$.

Asymptotic Expression:

Similar to Eq. (26), we define the asymptote for *scenario-2* in our proposed model to improve our analysis via extracting better intuitions. Making use of [Eq. (29), 71], asymptotic expression of Eq. (31) is derived as

$$\begin{aligned} SOP_{2,\infty} = & 1 - \mathcal{A} \sum_{N_0=1}^2 \sum_{v=0}^{\mu_0-1} \sum_{x=0}^{\mu_0-v-1} \frac{(\varphi_2 - 1)^x}{x!} e^{-l_{N_0}(\varphi_2-1)} l_{N_0}^x Y_{N_0,v} \{1 - \mathcal{B}_1 \mathcal{B}_5 \\ & \times \sum_{p=1}^{\delta_0} \frac{\prod_{h=1, h \neq p}^{\delta_0} \Gamma(\mathcal{J}_{1,p} - \mathcal{J}_{1,h}) \prod_{h=1}^{\delta_e+1} \Gamma(1 + \mathcal{J}_{2,h} - \mathcal{J}_{1,p})}{\prod_{h=\delta_0+1}^{s_e+\delta_0+1} \Gamma(1 + \mathcal{J}_{1,h} - \mathcal{J}_{1,p}) \prod_{h=\delta_e+2}^{s_0+\delta_e+1} \Gamma(\mathcal{J}_{1,p} - \mathcal{J}_{2,h})} \left[\frac{\mathcal{B}_6}{\mathcal{B}_4} \left(\frac{U_d}{U_e \varphi_2} \right)^\tau \right]^{\mathcal{J}_{1,p}-1} \Bigg\}, \end{aligned} \quad (32)$$

where $\mathcal{J}_1 = (1 - j_4, 1, j_5)$, and $\mathcal{J}_2 = (j_6, 0, 1 - j_3)$.

B. Strictly Positive Secrecy Capacity

The probability of SPSC is the inverse probable term of outage probability that is a positive volume of secrecy capacity. In this subsection, we derive expressions of SPSC for both scenarios described in Fig. 1.

B.1. scenario-1

Considering *scenario-1* wherein eavesdropper E_1 is located near the $S - R$ link, SPSC can be expressed as [72, 73]

$$\begin{aligned} SPSC_1 &= \Pr(\mathcal{T}_{D_1} > 0) \\ &= \Pr(\gamma_d > \gamma_{r_e}) \\ &= \int_0^\infty \int_0^{\gamma_d} f_d(\gamma_d) f_{r_e}(\gamma_{r_e}) d\gamma_{r_e} d\gamma_d \\ &= \int_0^\infty f_{\gamma_d}(\gamma) F_{\gamma_{r_e}}(\gamma) d\gamma. \end{aligned} \quad (33)$$

Substituting Eq. (13) and Eq. (19) into Eq. (33) and employing mathematical simplifications, SPSC for *scenario-1* is obtained as

$$\begin{aligned} SPSC_1 = & \mathcal{A} \sum_{N_0=1}^2 \sum_{v=0}^{\mu_0-1} \left\{ X_{N_0,v} \mathcal{R}_1 + \sum_{x=0}^{\mu_0-v-1} \frac{l_{N_0}^x}{x!} Y_{N_0,v} \mathcal{R}_2 - \mathcal{C} \sum_{N_e=1}^2 \sum_{w=0}^{\mu_e-1} \sum_{y=0}^{\mu_e-w-1} \frac{l_{N_e}^y}{y!} Y_{N_e,w} \right. \\ & \times \left. \left[X_{N_0,v} \mathcal{R}_3 + \sum_{x=0}^{\mu_0-v-1} \frac{l_{N_0}^x}{x!} Y_{N_0,v} \mathcal{R}_4 \right] \right\}, \end{aligned} \quad (34)$$

where \mathcal{R}_1 , \mathcal{R}_2 , \mathcal{R}_3 , and \mathcal{R}_4 are four integration terms. Now, Utilizing [eqs. (2.24.1.1) and (8.4.3.1), 69] \mathcal{R}_1 is obtained as

$$\begin{aligned} \mathcal{R}_1 &= \int_0^\infty \mathcal{B}_3 \gamma_d^{z_2-1} e^{-l_{N_0} \gamma_d} G_{s_0+1, \delta_0+1}^{\delta_0+1, 0} \left[\mathcal{B}_4 \left(\frac{\gamma_d}{U_d} \right)^\tau \middle| \begin{matrix} j_3, 1 \\ 0, j_4 \end{matrix} \right] d\gamma_d \\ &= \int_0^\infty \mathcal{B}_3 \gamma_d^{z_2-1} G_{0,1}^{1,0} \left[l_{N_0} \gamma_d \middle| \begin{matrix} - \\ 0 \end{matrix} \right] G_{s_0+1, \delta_0+1}^{\delta_0+1, 0} \left[\mathcal{B}_4 \left(\frac{\gamma_d}{U_d} \right)^\tau \middle| \begin{matrix} j_3, 1 \\ 0, j_4 \end{matrix} \right] d\gamma_d \\ &= \frac{\mathcal{B}_3}{l_{N_0}^{z_2}} G_{s_0+2, \delta_0+1}^{\delta_0+1, 1} \left[\mathcal{B}_4 \left(\frac{\tau}{U_d l_{N_0}} \right)^\tau \middle| \begin{matrix} 1 - z_2, j_3, 1 \\ 0, j_4 \end{matrix} \right], \end{aligned} \quad (35)$$

where $z_2 = \mu_0 - v$. The second integration term \mathcal{R}_2 is calculated similarly as

$$\begin{aligned}
\mathcal{R}_2 &= \int_0^\infty \frac{\mathcal{B}_1}{s_0} \gamma_d^{x-1} e^{-l_{N_0} \gamma_d} G_{1, \lambda_1 + \lambda_2 + 1}^{\lambda_1 + \lambda_2 + 1, 0} \left[\mathcal{B}_2 t^\tau \left(\frac{\gamma_d}{U_d} \right)^{\frac{\tau}{s_0}} \middle| \begin{matrix} j_2 \\ j_1 \end{matrix} \right] d\gamma_d \\
&= \int_0^\infty \mathcal{B}_1 s_0^{-1} \gamma_d^{x-1} G_{0,1}^{1,0} \left[l_{N_0} \gamma_d \middle| \begin{matrix} - \\ 0 \end{matrix} \right] G_{1, \lambda_1 + \lambda_2 + 1}^{\lambda_1 + \lambda_2 + 1, 0} \left[\mathcal{B}_2 t^\tau \left(\frac{\gamma_d}{U_d} \right)^{\frac{\tau}{s_0}} \middle| \begin{matrix} j_2 \\ j_1 \end{matrix} \right] d\gamma_d \\
&= \frac{\mathcal{B}_3}{l_{N_0}^x} G_{s_0+1, \delta_0}^{\delta_0, 1} \left[\mathcal{B}_4 \left(\frac{\tau}{U_d l_{N_0}} \right)^\tau \middle| \begin{matrix} 1-x, j_3 \\ j_4 \end{matrix} \right].
\end{aligned} \tag{36}$$

Performing identical mathematical calculations as \mathcal{R}_1 and \mathcal{R}_2 , \mathcal{R}_3 yields to

$$\begin{aligned}
\mathcal{R}_3 &= \int_0^\infty \mathcal{B}_3 \gamma_d^{z_3-1} e^{-\mathcal{H} \gamma_d} G_{s_0+1, \delta_0+1}^{\delta_0+1, 0} \left[\mathcal{B}_4 \left(\frac{\gamma_d}{U_d} \right)^\tau \middle| \begin{matrix} j_3, 1 \\ 0, j_4 \end{matrix} \right] d\gamma_d \\
&= \int_0^\infty \mathcal{B}_3 \gamma_d^{z_3-1} G_{0,1}^{1,0} \left[\mathcal{H} \gamma_d \middle| \begin{matrix} - \\ 0 \end{matrix} \right] G_{s_0+1, \delta_0+1}^{\delta_0+1, 0} \left[\mathcal{B}_4 \left(\frac{\gamma_d}{U_d} \right)^\tau \middle| \begin{matrix} j_3, 1 \\ 0, j_4 \end{matrix} \right] d\gamma_d \\
&= \frac{\mathcal{B}_3}{\mathcal{H}^{z_3}} G_{s_0+2, \delta_0+1}^{\delta_0+1, 1} \left[\mathcal{B}_4 \left(\frac{\tau}{U_d \mathcal{H}} \right)^\tau \middle| \begin{matrix} 1-z_3, j_3, 1 \\ 0, j_4 \end{matrix} \right],
\end{aligned} \tag{37}$$

where $\mathcal{H} = l_{N_0} + l_{N_e}$, and $z_3 = z_2 + y$. The last integration term \mathcal{R}_4 is obtained similarly as

$$\begin{aligned}
\mathcal{R}_4 &= \int_0^\infty \frac{\mathcal{B}_1}{s_0} \gamma_d^{z_4-1} e^{-\mathcal{H} \gamma_d} G_{1, \lambda_1 + \lambda_2 + 1}^{\lambda_1 + \lambda_2 + 1, 0} \left[\mathcal{B}_2 t^\tau \left(\frac{\gamma_d}{U_d} \right)^{\frac{\tau}{s_0}} \middle| \begin{matrix} j_2 \\ j_1 \end{matrix} \right] d\gamma_d \\
&= \int_0^\infty \mathcal{B}_1 s_0^{-1} \gamma_d^{z_4-1} G_{0,1}^{1,0} \left[\mathcal{H} \gamma_d \middle| \begin{matrix} - \\ 0 \end{matrix} \right] G_{1, \lambda_1 + \lambda_2 + 1}^{\lambda_1 + \lambda_2 + 1, 0} \left[\mathcal{B}_2 t^\tau \left(\frac{\gamma_d}{U_d} \right)^{\frac{\tau}{s_0}} \middle| \begin{matrix} j_2 \\ j_1 \end{matrix} \right] d\gamma_d \\
&= \frac{\mathcal{B}_3}{\mathcal{H}^{z_4}} G_{s_0+1, \delta_0}^{\delta_0, 1} \left[\mathcal{B}_4 \left(\frac{\tau}{U_d \mathcal{H}} \right)^\tau \middle| \begin{matrix} 1-z_4, j_3 \\ j_4 \end{matrix} \right],
\end{aligned} \tag{38}$$

where $z_4 = x + y$.

B.2. scenario-2

For the DF based system in *scenario-2*, SPSC can be defined as [Eq. (9), 74]

$$\begin{aligned}
\text{SPSC}_2 &= \Pr [\min(\mathcal{T}_S, \mathcal{T}_R) > 0] \\
&= \Pr (\mathcal{T}_S > 0) \Pr (\mathcal{T}_R > 0).
\end{aligned} \tag{39}$$

For $S - R$ link, in the case of *scenario-2*, the positive probability term is expressed as

$$\begin{aligned}
\Pr (\mathcal{T}_S > 0) &= \Pr \left[\frac{1}{2} \log_2(1 + \gamma_{r_0}) > 0 \right] \\
&= \Pr (\gamma_{r_0} > 0) \\
&= 1.
\end{aligned} \tag{40}$$

For second-hop, the probability term is defined as

$$\begin{aligned}\Pr(\mathcal{T}_R > 0) &= \Pr\left\{\frac{1}{2}[\log_2(1 + \gamma_{d_0}) - \log_2(1 + \gamma_{d_e})] > 0\right\} \\ &= \Pr(\gamma_{d_0} > \gamma_{d_e}) \\ &= 1 - \int_0^\infty F_{\gamma_{d_0}}(\gamma) f_{\gamma_{d_e}}(\gamma) d\gamma.\end{aligned}\quad (41)$$

Substituting Eq. (40) and Eq. (41) into Eq. (39), the SPSC can be denoted as

$$SPSC_2 = 1 - \int_0^\infty F_{\gamma_{d_0}}(\gamma) f_{\gamma_{d_e}}(\gamma) d\gamma. \quad (42)$$

Setting the values of Eq. (10) and Eq. (14) into Eq. (42), and performing integration utilizing [Eq. (2.24.1.1), 69], Eq. (42) is obtained as

$$SPSC_2 = 1 - \mathcal{B}_3 \mathcal{B}_5 G_{s_e + \delta_0 + 1, s_0 + \delta_e + 1}^{\delta_e + 1, \delta_0} \left[\frac{\mathcal{B}_6}{\mathcal{B}_4} \left(\frac{U_d}{U_e} \right)^\tau \middle| \begin{matrix} 1 - j_4, 1, j_5 \\ j_6, 0, 1 - j_3 \end{matrix} \right]. \quad (43)$$

It can be noted that by setting the fading parameter values to $\eta_0 = 1, \mu_0 = 1$ and $a_1 = a_2 = \Omega_1 = \Omega_2 = 1$, the expression derived in Eq. (43) matches with [Eq. (23), 51] of the Rayleigh-IT fading distribution.

4. NUMERICAL RESULTS

In this section, we present some analytical results utilizing the derived expressions of the secrecy metrics, namely lower bound and asymptotic SOP, and SPSC to demonstrate the impact of the system parameters on secrecy performance considering both eavesdropping scenarios. To corroborate our analytical outcomes, we also demonstrate Monte-Carlo simulations via generating $\eta - \mu$ and DGG random variables in MATLAB and averaging 100,000 channel realizations to acquire each value of the secrecy parameters. It is noteworthy

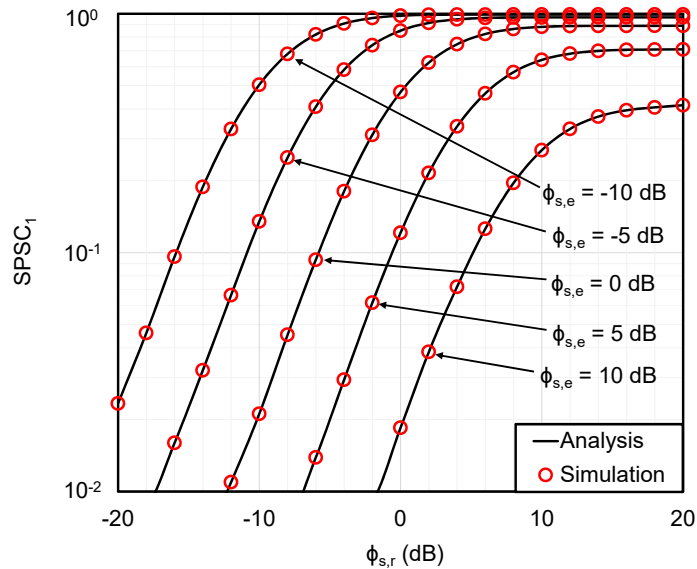


Fig. 2. The $SPSC_1$ versus $\phi_{s,r}$ for selected values of $\phi_{s,e}$ with $\eta_0 = \eta_e = 20, \mu_0 = \mu_e = 2, a_1 = a_2 = 2.1, b_1 = 4, b_2 = 4.5, \Omega_1 = 1.07, \Omega_2 = 1.06, \lambda_1 = \lambda_2 = 1, s_0 = 1, U_d = 10$ dB, and $\epsilon = 1$.

in figures that the analytical and simulation results are in good agreement with each other. The analysis is performed by assuming some parametric values such as $\eta_0 \geq 0$, $\eta_e \geq 0$, $\mu_0 \geq 0$, $\mu_e \geq 0$, $\mathcal{T}_{D_1} = \mathcal{T}_{D_2} = 1$, $\mathcal{T}_{C_1} = \mathcal{T}_{C_2} = 0.5$ bits/sec/Hz, $s_0 = s_e = (1, 2)$, and $\epsilon = \{1, 6.7\}$. To analyze natural turbulence levels over the DGG link, we set up the following values for atmospheric turbulence parameters [54].

- $a_1 = 1.86$, $a_2 = 1$, $b_1 = 0.5$, $b_2 = 1.8$, $\Omega_1 = 1.51$, $\Omega_2 = 1$, $\lambda_1 = 17$, and $\lambda_2 = 9$ for strong turbulence (ST).
- $a_1 = 2.17$, $a_2 = 1$, $b_1 = 0.55$, $b_2 = 2.35$, $\Omega_1 = 1.58$, $\Omega_2 = 0.97$, $\lambda_1 = 28$, and $\lambda_2 = 13$ for moderate turbulence (MT).
- $a_1 = a_2 = 2.1$, $b_1 = 4$, $b_2 = 4.5$, $\Omega_1 = 1.07$, $\Omega_2 = 1.06$, and $\lambda_1 = \lambda_2 = 1$ for weak turbulence (WT).

The impact of average SNR of the eavesdropper links on the secrecy performance is investigated in Figs. 2 and 3.

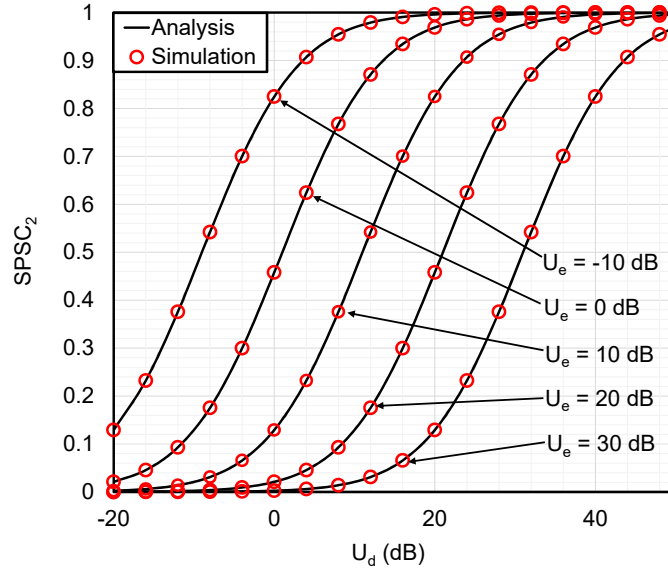


Fig. 3. The SPSC_2 versus U_d for selected values of U_e with $a_1 = 1.86$, $a_2 = 1$, $b_1 = 0.5$, $b_2 = 1.8$, $\Omega_1 = 1.51$, $\Omega_2 = 1$, $\lambda_1 = 17$, $\lambda_2 = 9$, $s_0 = s_e = 1$, and $\epsilon = 1$.

Fig. 2 indicates relationship between SPSC_1 and $\phi_{s,r}$ i.e. the first scenario. It is observed SPSC_1 increases when the average SNR of $S - E_1$ link $\phi_{s,e}$ decreases from 10 dB to -10 dB. On the other hand, Fig. 3 illustrates the effect of average SNR of $R - E_2$ link, i.e., the second scenario. This time U_e is decreased from 30 dB to -10 dB. As a result, the performance metric SPSC_2 that is plotted against U_d , increases remarkably. These two events reveal that decrease in $\phi_{s,e}$ and U_e renders the eavesdropper channels weaker relative to the main channel thereby the SPSC performance improves as reported in [49, 75].

A comparative analysis between two types of detection techniques at the receiver is demonstrated in Figs. 4-6 where all the figures are plotted against U_d . Figs. 4 and 5 demonstrate this comparison under *Scenario-1* while Fig. 6 illustrates the same under *Scenario-2*. Results imply that utilizing HD technique ($s_0 = s_e = 1$) for signal detection provides better secrecy output relative to IM/DD technique ($s_0 = s_e = 2$). The reason behind these outcomes is that HD technique provides higher SNR than IM/DD technique at the destination receiver. The results demonstrated in [45, 51] also agree with our demonstrated results that validates our analysis.

The influence of pointing errors in FSO links is demonstrated in Figs. 7-9. Fig. 7 illustrates SOP_1 vs $\phi_{s,r}$ applicable to *scenario-1*, and Figs. 8 and 9 demonstrates SOP_2 and SPSC_2 , respectively, plotted against U_d applicable to *scenario-2*. All three figures demonstrate that the secrecy performance for both eavesdropping

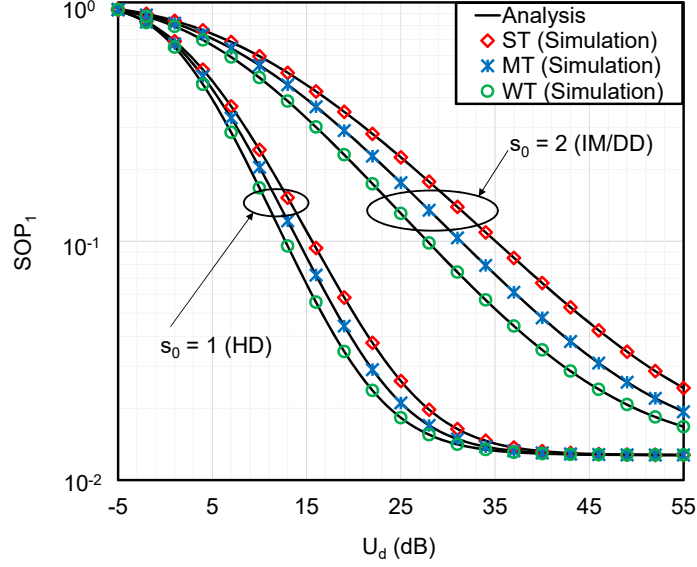


Fig. 4. The SOP_1 versus U_d for selected values of $s_0, a_1, a_2, b_1, b_2, \Omega_1, \Omega_2, \lambda_1$, and λ_2 with $\eta_0 = \eta_e = 50$, $\mu_0 = \mu_e = 3$, $\phi_{s,r} = 10$ dB, $\phi_{s,e} = 0$ dB, and $\epsilon = 1$.

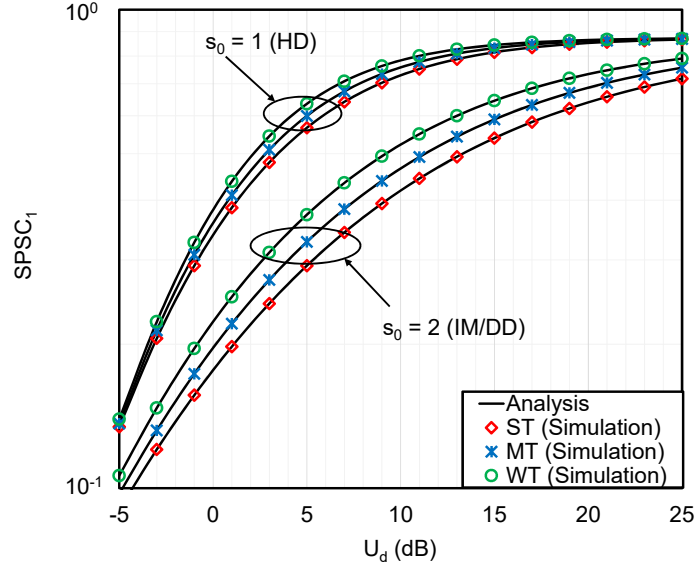


Fig. 5. The $SPSC_1$ versus U_d for selected values of $s_0, a_1, a_2, b_1, b_2, \Omega_1, \Omega_2, \lambda_1$, and λ_2 with $\eta_0 = \eta_e = 25$, $\mu_0 = \mu_e = 2$, $\phi_{s,r} = 5$ dB, $\phi_{s,e} = 0$ dB, and $\epsilon = 1$.

scenarios increases when DGG main link undergoes from severe pointing error ($\epsilon=1$) to negligible pointing error ($\epsilon=6.7$). Similar outcomes were demonstrated in [41, 51] that corroborate our investigations. Besides, asymptotic outputs are demonstrated in Figs. 7 and 8 for SOP_1 and SOP_2 , respectively, that reveal the asymptotic lower bound SOP results can tightly approximate our derived lower bound SOP results in high SNR regime.

Besides the detection technique types and pointing errors, the turbulence parameters of DGG channel also

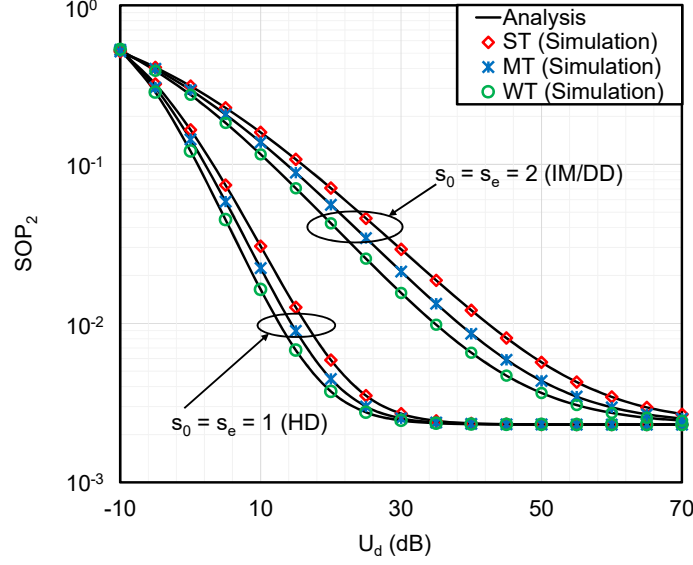


Fig. 6. The SOP_2 versus U_d for selected values of $s_0, s_e, a_1, a_2, b_1, b_2, \Omega_1, \Omega_2, \lambda_1$, and λ_2 with $\eta_0 = 5, \mu_0 = 1, \phi_{s,r} = 12$ dB, $U_e = -10$ dB, and $\epsilon = 1$.

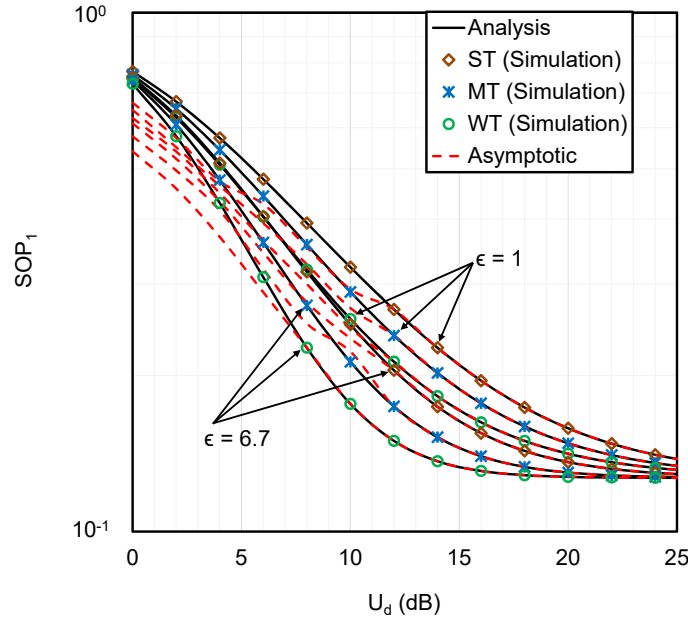


Fig. 7. The SOP_1 versus U_d for selected values of $\epsilon, a_1, a_2, b_1, b_2, \Omega_1, \Omega_2, \lambda_1$, and λ_2 with $\eta_0 = \eta_e = 25, \mu_0 = \mu_e = 4, \phi_{s,r} = 5$ dB, $\phi_{s,e} = 0$ dB, and $s_0 = 1$.

place notable influences on the secrecy performance. Figs. 4-9 indicate the effects of three turbulence conditions, namely, ST, MT, and WT. Our demonstrated outcomes show the expected results similar to [41, 45, 51] that secrecy performance with weaker turbulence in Figs. 4-9 clearly outperforms that under stronger turbulence.

Generalization Demonstrated via the Proposed Model:

In this proposed model, we assume $\eta - \mu$ fading model over the RF hop and DGG turbulence model over

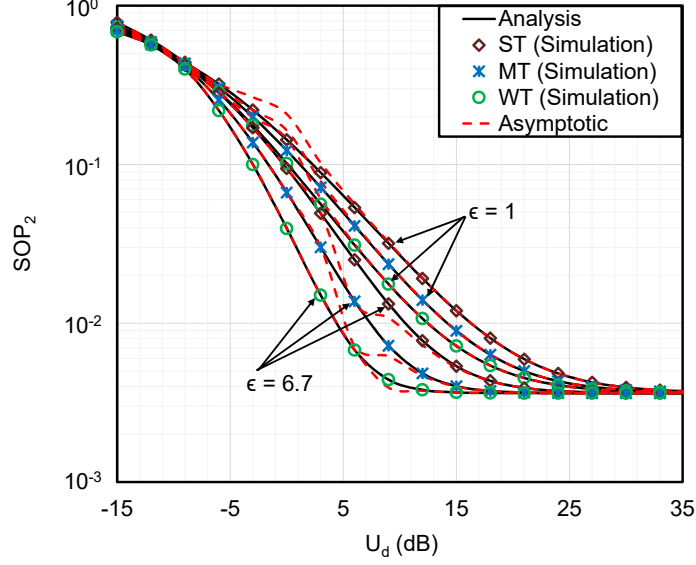


Fig. 8. The SOP_2 versus U_d for selected values of ϵ , a_1 , a_2 , b_1 , b_2 , Ω_1 , Ω_2 , λ_1 , and λ_2 with $\eta_0 = 2$, $\mu_0 = 1$, $\phi_{s,r} = 10$ dB, $s_0 = s_e = 1$, and $U_e = -12$ dB.

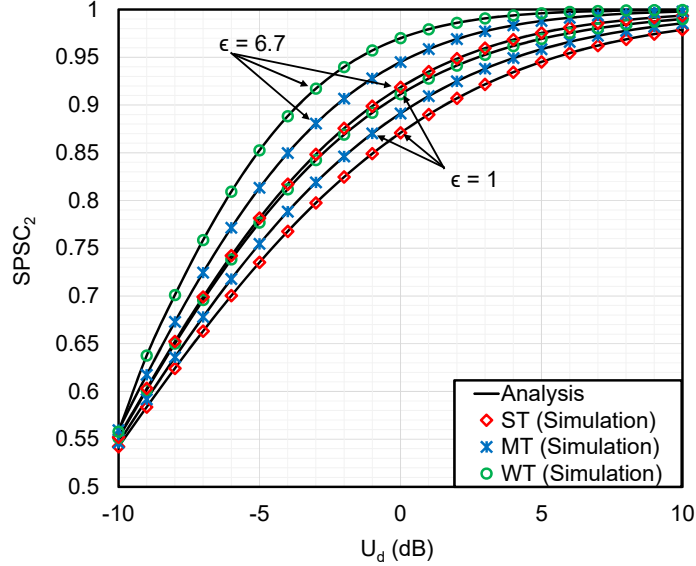


Fig. 9. The $SPSC_2$ versus U_d for selected values of ϵ , a_1 , a_2 , b_1 , b_2 , Ω_1 , Ω_2 , λ_1 , and λ_2 with $s_0 = s_e = 1$ and $U_e = -10$ dB.

the FSO hop. The $\eta - \mu$ distribution has an outstanding generic nature that can emerge several multipath fading channels as special cases that are indicated in Table 1. On the other hand, DGG turbulence model is also regarded as a generalized FSO turbulent model from which multiple classical FSO models can be generated as special cases, as listed in Table 2. It can be clearly observed the demonstrated channel models indicated in [41] and [44] can be addressed as the special cases of *scenario-1*. Likewise, the secure models denoted in [51] can be addressed as a special case of our proposed *scenario-2*. Subsequently, Table 3 summarizes some other special

Table 3. Some researches as Special Cases of Our Proposed Model

Reference	RF link	FSO link	Eavesdropper link
-	Rayleigh ($\eta = 1, \mu = 1$)	K distribution ($a_1 = a_2 = b_1 = \Omega_1 = \Omega_2 = \lambda_1 = \lambda_2 = 1, b_2 = 1.8$)	-
-	Rayleigh ($\eta = 1, \mu = 1$)	Double Weibull ($a_1 = a_2 = 2.1, b_1 = b_2 = 1, \Omega_1 = 1.07, \Omega_2 = 1.06, \lambda_1 = \lambda_2 = 1$)	-
-	Nakagami- m ($\eta = 20, \mu = 2$)	Log-normal ($a_1 = a_2 = 0.01, b_1 = 4, b_2 = 4.5, \Omega_1 = \Omega_2 = 1.07, \lambda_1 = \lambda_2 = 1$)	-
[27]	Nakagami- m ($\eta = 20, \mu = 2$)	DGG ($a_1 = 2.17, a_2 = 1, b_1 = 0.55, b_2 = 2.35, \Omega_1 = 1.58, \Omega_2 = 0.97, \lambda_1 = 28, \lambda_2 = 13$)	-
[32]	$\eta - \mu$ ($\eta = 100, \mu = 2$)	$\Gamma\Gamma$ ($a_1 = a_2 = \Omega_1 = \Omega_2 = \lambda_1 = \lambda_2 = 1, b_1 = 2.296, b_2 = 1.822$)	-
[41]	Nakagami- m ($\eta = 20, \mu = 2$)	$\Gamma\Gamma$ ($a_1 = a_2 = \Omega_1 = \Omega_2 = \lambda_1 = \lambda_2 = 1, b_1 = 2.296, b_2 = 1.822$)	RF
[44]	Rayleigh ($\eta = 1, \mu = 1$)	$\Gamma\Gamma$ ($a_1 = a_2 = \Omega_1 = \Omega_2 = \lambda_1 = \lambda_2 = 1, b_1 = 2.296, b_2 = 1.822$)	RF
[51]	Rayleigh ($\eta = 1, \mu = 1$)	$\Gamma\Gamma$ ($a_1 = a_2 = \Omega_1 = \Omega_2 = \lambda_1 = \lambda_2 = 1, b_1 = 2.296, b_2 = 1.822$)	FSO

cases that are not available in the literature till date and these are graphically represented in Figs. 10 and 11.

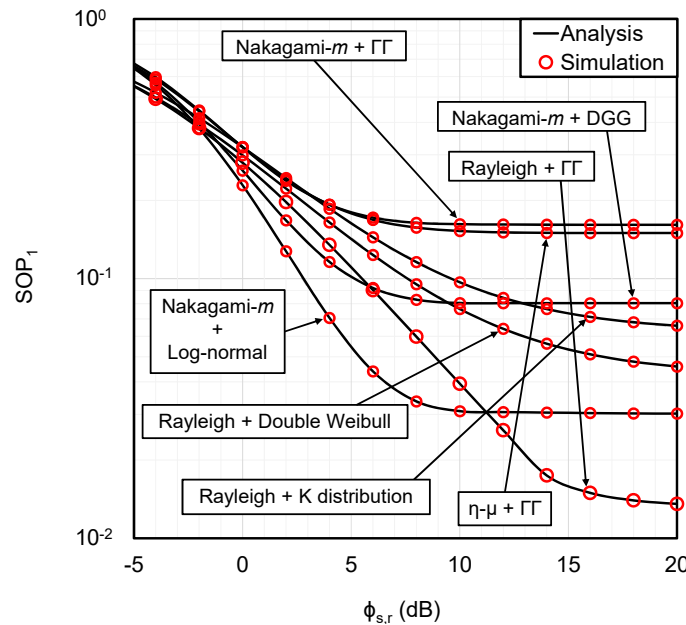


Fig. 10. The SOP_1 versus $\phi_{s,r}$ for selected values of $\eta_0, \eta_e, \mu_0, \mu_e, a_1, a_2, b_1, b_2, \Omega_1, \Omega_2, \lambda_1$, and λ_2 with $\phi_{s,e} = -5$ dB, $s_0 = 1$, $U_d = 5$ dB, and $\epsilon = 6.7$.

Hence, we can express that existing researches in [41, 44, 51] can be obtained as the special cases of our model that clearly demonstrates the novelty and supremacy of our model relative to the existing literature.

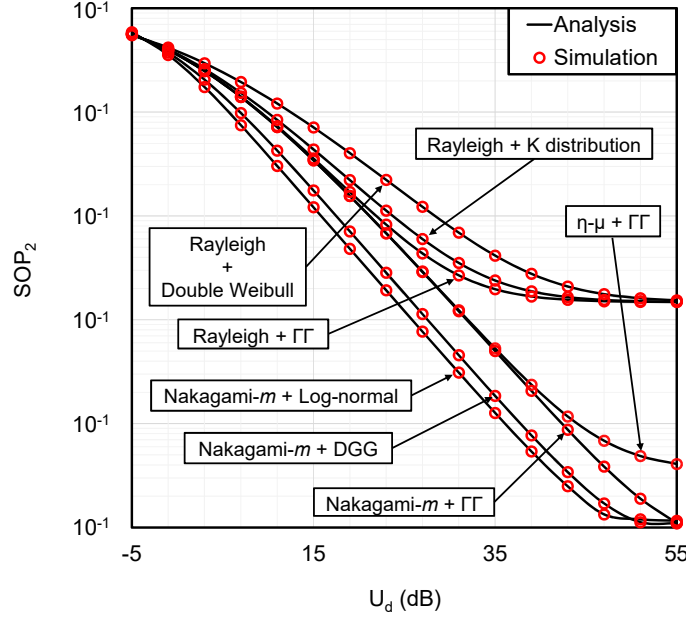


Fig. 11. The SOP_2 versus U_d for selected values of $\eta_0, \mu_0, a_1, a_2, b_1, b_2, \Omega_1, \Omega_2, \lambda_1$, and λ_2 with $\phi_{s,r} = 12$ dB, $s_0 = s_e = 1$, $U_e = -5$ dB, and $\epsilon = 1$.

5. CONCLUSION

This paper analyses the secrecy performance of an RF-FSO mixed framework under eavesdropping attempts via the RF or FSO links. The RF hop experiences $\eta - \mu$ fading channel whereas the FSO hop undergoes unified DGG turbulence with pointing error impairments. The secrecy analyses are performed deducing expressions for SPSC and SOP in closed-form and obtaining further useful insights via deriving asymptotic SOP expressions. All the analytical expressions are also verified via MC simulations. Utilizing the derived expressions, impacts of fading, weak to strong atmospheric turbulences, and pointing errors are also observed. It is seen that our demonstrated results exhibit a generalization of the various reported outcomes in the literature. Moreover, a comparison between HD and IM/DD techniques reveals the HD technique offers a better and secure outage performance over the proposed scheme relative to the IM/DD technique.

REFERENCES

1. X. Zhu and J. M. Kahn, "Free-space optical communication through atmospheric turbulence channels," *IEEE Transactions on communications* **50**, 1293–1300 (2002).
2. S. M. Haas and J. H. Shapiro, "Capacity of wireless optical communications," *IEEE J. on Sel. Areas communications* **21**, 1346–1357 (2003).
3. A. A. Farid and S. Hranilovic, "Outage capacity optimization for free-space optical links with pointing errors," *J. Light. technology* **25**, 1702–1710 (2007).
4. A. Belmonte and J. M. Kahn, "Capacity of coherent free-space optical links using diversity-combining techniques," *Opt. express* **17**, 12601–12611 (2009).
5. E. Bayaki, R. Schober, and R. K. Mallik, "Performance analysis of MIMO free-space optical systems in Gamma-Gamma fading," *IEEE Transactions on Commun.* **57**, 3415–3424 (2009).
6. A. A. Farid and S. Hranilovic, "Diversity gain and outage probability for MIMO free-space optical links with misalignment," *IEEE Transactions on Commun.* **60**, 479–487 (2011).
7. I. S. Ansari, M.-S. Alouini, and J. Cheng, "Ergodic capacity analysis of free-space optical links with nonzero boresight pointing errors," *IEEE Transactions on Wirel. Commun.* **14**, 4248–4264 (2015).
8. I. S. Ansari, F. Yilmaz, and M.-S. Alouini, "Performance analysis of free-space optical links over Málaga (\mathcal{M}) turbulence channels with pointing errors," *IEEE Transactions on Wirel. Commun.* **15**, 91–102 (2015).
9. M. Safari and M. Uysal, "Relay-assisted free-space optical communication," *IEEE Transactions on Wirel. Commun.* **7**, 5441–5449 (2008).
10. R. Boluda-Ruiz, A. García-Zambrana, B. Castillo-Vázquez, and C. Castillo-Vázquez, "Ergodic capacity analysis of decode-and-forward relay-assisted FSO systems over Alpha-Mu fading channels considering pointing errors," *IEEE Photonics J.* **8**, 1–11 (2015).
11. L. Yang, M.-S. Alouini, and I. S. Ansari, "Asymptotic performance analysis of two-way relaying FSO networks with nonzero boresight pointing errors over double-generalized gamma fading channels," *IEEE Transactions on Veh. Technol.* **67**, 7800–7805 (2018).
12. J. Gupta, V. K. Dwivedi, and V. Karwal, "On the performance of RF-FSO system over Rayleigh and Kappa-Mu/Inverse Gaussian fading environment," *IEEE Access* **6**, 4186–4198 (2018).

13. I. S. Ansari, M. M. Abdallah, M. Alouini, and K. A. Qaraqe, "A performance study of two hop transmission in mixed underlay RF and FSO fading channels," in *2014 IEEE Wireless Communications and Networking Conference (WCNC)*, (2014), pp. 388–393.
14. J. Vellakudiyan, I. S. Ansari, V. Palliyembil, P. Muthuchidambaranathan, and K. A. Qaraqe, "Channel capacity analysis of a mixed dual-hop radio-frequency-free space optical transmission system with Málaga distribution," *IET Commun.* **10**, 2119–2124 (2016).
15. J. Vellakudiyan, V. Palliyembil, I. S. Ansari, P. Muthuchidambaranathan, and K. A. Qaraqe, "Performance analysis of the decode-and-forward relay-based RF-FSO communication system in the presence of pointing errors," *IET Signal Process.* **13**, 480–485 (2019).
16. F. S. Al-Qahtani, A. H. A. El-Malek, I. S. Ansari, R. M. Radaydeh, and S. A. Zummo, "Outage analysis of mixed underlay cognitive RF MIMO and FSO relaying with interference reduction," *IEEE Photonics J.* **9**, 1–22 (2017).
17. Y. F. Al-Eryani, A. M. Salhab, S. A. Zummo, and M.-S. Alouini, "Two-way multiuser mixed RF/FSO relaying: Performance analysis and power allocation," *J. Opt. Commun. Netw.* **10**, 396–408 (2018).
18. M. I. Petkovic and Z. Trpovski, "Exact outage probability analysis of the mixed RF/FSO system with variable-gain relays," *IEEE Photonics J.* **10**, 1–14 (2018).
19. L. Yang, M. O. Hasna, and X. Gao, "Performance of mixed RF/FSO with variable gain over generalized atmospheric turbulence channels," *IEEE J. on Sel. Areas Commun.* **33**, 1913–1924 (2015).
20. E. Balti, M. Guizani, B. Hamdaoui, and B. Khalfi, "Aggregate hardware impairments over mixed RF/FSO relaying systems with outdated CSI," *IEEE Transactions on Commun.* **66**, 1110–1123 (2017).
21. G. T. Djordjevic, M. I. Petkovic, A. M. Cvetkovic, and G. K. Karagiannidis, "Mixed RF/FSO relaying with outdated channel state information," *IEEE J. on selected areas Commun.* **33**, 1935–1948 (2015).
22. A. M. Salhab, F. S. Al-Qahtani, R. M. Radaydeh, S. A. Zummo, and H. Alnuweiri, "Power allocation and performance of multiuser mixed RF/FSO relay networks with opportunistic scheduling and outdated channel information," *J. Light. Technol.* **34**, 3259–3272 (2016).
23. I. S. Ansari, M. M. Abdallah, M. Alouini, and K. A. Qaraqe, "Outage analysis of asymmetric RF-FSO systems," in *2016 IEEE 84th Vehicular Technology Conference (VTC-Fall)*, (2016), pp. 1–6.
24. O. M. S. Al-Ebraheemy, A. M. Salhab, A. Chaaban, S. A. Zummo, and M.-S. Alouini, "Precise performance analysis of dual-hop mixed RF/unified-FSO DF relaying with heterodyne detection and two IM-DD channel models," *IEEE Photonics J.* **11**, 1–22 (2019).
25. S. Anees and M. R. Bhatnagar, "Performance of an amplify-and-forward dual-hop asymmetric RF-FSO communication system," *J. Opt. Commun. Netw.* **7**, 124–135 (2015).
26. E. Zedini, I. S. Ansari, and M.-S. Alouini, "Performance analysis of mixed Nakagami- m and Gamma-Gamma dual-hop FSO transmission systems," *IEEE Photonics J.* **7**, 1–20 (2014).
27. D. R. Pattanayak, S. Rai, V. K. Dwivedi, and G. Singh, "A statistical channel model for a decode-and-forward based dual hop mixed RF/FSO relay network," *Opt. Quantum Electron.* **50**, 1–17 (2018).
28. V. Palliyembil, J. Vellakudiyan, P. Muthuchidambaranathan, and T. A. Tsiftsis, "Capacity and outage probability analysis of asymmetric dual-hop RF-FSO communication systems," *IET Commun.* **12**, 1979–1983 (2018).
29. I. S. Ansari and M. Alouini, "Asymptotic ergodic capacity analysis of composite Lognormal shadowed channels," in *2015 IEEE 81st Vehicular Technology Conference (VTC Spring)*, (2015), pp. 1–5.
30. H. Arezumand, H. Zamiri-Jafarian, and E. Soleimani-Nasab, "Outage and diversity analysis of underlay cognitive mixed RF-FSO cooperative systems," *J. Opt. Commun. Netw.* **9**, 909–920 (2017).
31. E. Soleimani-Nasab and M. Uysal, "Generalized performance analysis of mixed RF/FSO cooperative systems," *IEEE Transactions on Wirel. Commun.* **15**, 714–727 (2015).
32. N. Sharma, A. Bansal, and P. Garg, "Decode-and-forward relaying in mixed η - μ and Gamma-Gamma dual hop transmission system," *IET Commun.* **10**, 1769–1776 (2016).
33. I. S. Ansari, M. Alouini, and J. Cheng, "On the capacity of FSO links under Lognormal and Rician-Lognormal turbulences," in *2014 IEEE 80th Vehicular Technology Conference (VTC2014-Fall)*, (2014), pp. 1–6.
34. L. Yang, M. O. Hasna, and I. S. Ansari, "Unified performance analysis for multiuser mixed η - μ and \mathcal{M} -distribution dual-hop RF/FSO systems," *IEEE Transactions on Commun.* **65**, 3601–3613 (2017).
35. J. Zhang, L. Dai, Y. Zhang, and Z. Wang, "Unified performance analysis of mixed radio frequency/free-space optical dual-hop transmission systems," *J. Light. Technol.* **33**, 2286–2293 (2015).
36. I. S. Ansari and M. Alouini, "On the performance analysis of digital communications over Weibull-Gamma channels," in *2015 IEEE 81st Vehicular Technology Conference (VTC Spring)*, (2015), pp. 1–7.
37. A. Upadhyay, V. K. Dwivedi, and G. K. Karagiannidis, "On the effect of interference and misalignment error in mixed RF/FSO systems over generalized fading channels," *IEEE Transactions on Commun.* (2020).
38. I. S. Ansari, "Composite and cascaded Generalized-K fading channel modeling and their diversity and performance analysis," (2010).
39. S. H. Islam, A. Badrudduza, S. R. Islam, F. I. Shahid, I. S. Ansari, M. K. Kundu, and H. Yu, "Impact of correlation and pointing error on secure outage performance over arbitrary correlated Nakagami- m and \mathcal{M} -turbulent fading mixed RF-FSO channel," *IEEE Photonics J.* **13**, 1–17 (2021).
40. F. J. Lopez-Martinez, G. Gomez, and J. M. Garrido-Balsells, "Physical-layer security in free-space optical communications," *IEEE Photonics J.* **7**, 1–14 (2015).
41. H. Lei, Z. Dai, I. S. Ansari, K.-H. Park, G. Pan, and M.-S. Alouini, "On secrecy performance of mixed RF-FSO systems," *IEEE Photonics J.* **9**, 1–14 (2017).
42. L. Yang, T. Liu, J. Chen, and M.-S. Alouini, "Physical-layer security for mixed η - μ and \mathcal{M} -distribution dual-hop RF/FSO systems," *IEEE Transactions on Veh. Technol.* **67**, 12427–12431 (2018).
43. N. S. Mandira, M. K. Kundu, S. H. Islam, A. Badrudduza, and I. S. Ansari, "On secrecy performance of mixed α - η - μ and Málaga RF-FSO variable gain relaying channel," *arXiv preprint arXiv:2105.12265* (2021).
44. A. H. Abd El-Malek, A. M. Salhab, S. A. Zummo, and M.-S. Alouini, "Physical layer security enhancement in multiuser mixed RF/FSO relay networks under RF interference," in *2017 IEEE Wireless Communications and Networking Conference (WCNC)*, (IEEE, 2017), pp. 1–6.
45. H. Lei, H. Luo, K.-H. Park, Z. Ren, G. Pan, and M.-S. Alouini, "Secrecy outage analysis of mixed RF-FSO systems with channel imperfection," *IEEE Photonics J.* **10**, 1–13 (2018).
46. H. Lei, Z. Dai, K.-H. Park, W. Lei, G. Pan, and M.-S. Alouini, "Secrecy outage analysis of mixed RF-FSO downlink SWIPT systems," *IEEE Transactions on Commun.* **66**, 6384–6395 (2018).
47. M. J. Saber, A. Keshavarz, J. Mazloum, A. M. Sazdar, and M. J. Piran, "Physical-layer security analysis of mixed SIMO SWIPT RF and FSO fixed-gain

relaying systems," IEEE Syst. J. **13**, 2851–2858 (2019).

48. S. H. Islam, A. Badrudduza, S. R. Islam, F. I. Shahid, I. S. Ansari, M. K. Kundu, S. K. Ghosh, M. B. Hossain, A. S. Hosen, and G. H. Cho, "On secrecy performance of mixed Generalized Gamma and Málaga RF-FSO variable gain relaying channel," IEEE Access (2020).
49. N. A. Sarker, A. Badrudduza, S. R. Islam, S. H. Islam, I. S. Ansari, M. K. Kundu, M. F. Samad, M. B. Hossain, and H. Yu, "Secrecy performance analysis of mixed hyper-Gamma and Gamma-Gamma cooperative relaying system," IEEE Access **8**, 131273–131285 (2020).
50. H. Lei, H. Luo, K.-H. Park, I. S. Ansari, W. Lei, G. Pan, and M.-S. Alouini, "On secure mixed RF-FSO systems with TAS and imperfect CSI," IEEE Transactions on Commun. (2020).
51. X. Pan, H. Ran, G. Pan, Y. Xie, and J. Zhang, "On secrecy analysis of DF based dual hop mixed RF-FSO systems," IEEE Access **7**, 66725–66730 (2019).
52. H. AlQuwaiee, I. S. Ansari, and M.-S. Alouini, "On the performance of free-space optical communication systems over double generalized gamma channel," IEEE journal on selected areas communications **33**, 1829–1840 (2015).
53. N. D. Chatzidihamantis, H. G. Sandalidis, G. K. Karagiannidis, S. A. Kotsopoulos, and M. Matthaiou, "New results on turbulence modeling for free-space optical systems," in *2010 17th International Conference on Telecommunications*, (IEEE, 2010), pp. 487–492.
54. M. A. Kashani, M. Uysal, and M. Kavehrad, "A novel statistical channel model for turbulence-induced fading in free-space optical systems," J. Light. Technol. **33**, 2303–2312 (2015).
55. M. D. Yacoub, "The $\kappa - \mu$ distribution and the $\eta - \mu$ distribution," IEEE Antennas Propag. Mag. **49**, 68–81 (2007).
56. M. O. Hasna and M.-S. Alouini, "A performance study of dual-hop transmissions with fixed gain relays," IEEE transactions on wireless communications **3**, 1963–1968 (2004).
57. M. Z. I. Sarkar and T. Ratnarajah, "Enhancing security in correlated channel with maximal ratio combining diversity," IEEE transactions on signal processing **60**, 6745–6751 (2012).
58. Y. Ai, A. Mathur, M. Cheffena, M. R. Bhatnagar, and H. Lei, "Physical layer security of hybrid satellite-FSO cooperative systems," IEEE Photonics J. **11**, 1–14 (2019).
59. D. B. Da Costa and M. D. Yacoub, "Average channel capacity for generalized fading scenarios," IEEE Commun. Lett. **11**, 949–951 (2007).
60. I. S. Ansari, F. Yilmaz, and M. Alouini, "On the sum of squared $\eta - \mu$ random variates with application to the performance of wireless communication systems," in *2013 IEEE 77th Vehicular Technology Conference (VTC Spring)*, (2013), pp. 1–6.
61. I. S. Gradshteyn and I. M. Ryzhik, *Table of integrals, series, and products* (Academic press, 2014).
62. A. Al-Habash, L. C. Andrews, and R. L. Phillips, "Mathematical model for the irradiance probability density function of a laser beam propagating through turbulent media," Opt. engineering **40**, 1554–1563 (2001).
63. T. A. Tsiftsis, H. G. Sandalidis, G. K. Karagiannidis, and M. Uysal, "Optical wireless links with spatial diversity over strong atmospheric turbulence channels," IEEE Transactions on Wirel. Commun. **8**, 951–957 (2009).
64. M. Niu, J. Cheng, and J. F. Holzman, "Error rate performance comparison of coherent and subcarrier intensity modulated optical wireless communications," J. Opt. Commun. Netw. **5**, 554–564 (2013).
65. H. Lei, H. Zhang, I. S. Ansari, C. Gao, Y. Guo, G. Pan, and K. A. Qaraqe, "Performance analysis of physical layer security over generalized- k fading channels using a mixture Gamma distribution," IEEE Commun. Lett. **20**, 408–411 (2015).
66. A. S. Sumona, M. K. Kundu, and A. Badrudduza, "Security analysis in multicasting over shadowed rician and $\alpha - \mu$ fading channels: A dual-hop hybrid satellite terrestrial relaying network," arXiv preprint arXiv:2105.12071 (2021).
67. A. Badrudduza, M. Ibrahim, S. R. Islam, M. S. Hossen, M. K. Kundu, I. S. Ansari, and H. Yu, "Security at the physical layer over GG fading and mEGG turbulence induced RF-UOWC mixed system," IEEE Access **9**, 18123–18136 (2021).
68. H. Lei, C. Gao, Y. Guo, and G. Pan, "On physical layer security over Generalized Gamma fading channels," IEEE Commun. Lett. **19**, 1257–1260 (2015).
69. A. Prudnikov, Y. Brychkov, and O. Marichev, *Integrals and Series: More special functions*, vol. 3 (Gordon And Breach Science Publishers, 1992).
70. M. D. Springer, "The algebra of random variables," Tech. rep. (1979).
71. D. R. Pattanayak, V. K. Dwivedi, and V. Karwal, "Physical layer security of a two way relay based mixed FSO/RF network in the presence of multiple eavesdroppers," Opt. Commun. **463**, 125429 (2020).
72. A. Badrudduza, M. Sarkar, and M. K. Kundu, "Enhancing security in multicasting through correlated Nakagami-m fading channels with opportunistic relaying," Phys. Commun. **43**, 101177 (2020).
73. M. Ibrahim, A. Badrudduza, M. Hossen, M. K. Kundu, I. S. Ansari *et al.*, "Enhancing security of TAS/MRC based mixed RF-UOWC system with induced underwater turbulence effect," arXiv preprint arXiv:2105.09088 (2021).
74. X. Liu, "Probability of strictly positive secrecy capacity of the Rician-Rician fading channel," IEEE Wirel. Commun. Lett. **2**, 50–53 (2012).
75. N. H. Juel, A. Badrudduza, S. R. Islam, S. H. Islam, M. kumar Kundu, I. S. Ansari, M. M. Mowla, and K.-S. Kwak, "Secrecy performance analysis of mixed $\alpha - \mu$ and Exponentiated Weibull RF-FSO cooperative relaying system," IEEE Access (2021).